



Extraction information of moiré fringes based on Gabor wavelet

Ya-yi Chen^{1,3,4} · Yun-yun Chen^{1,2,3,4} · Wei-hao Cheng^{1,3,4} · Meng Xu^{1,3,4} · Jun-yan Zhuang^{1,3,4}

Received: 17 November 2021 / Accepted: 5 April 2022 / Published online: 28 April 2022
© The Optical Society of Japan 2022

Abstract

In the process of extracting information from the moiré fringes, phase information extraction is one of the crucial means. In this paper, Gabor wavelet transform method is proposed to extract phase information of moiré fringes. First, the light intensity of first-ordered moiré fringe is selected to derive the phase based on the Gabor wavelet transform method. Then, to prove that our method is feasible, three flow fields are adopted for experiment, whose phase information is successfully extracted. Finally, the phase information results above are compared with those extracted by Fourier transform method, which proves that the Gabor wavelet transform method has an advantage in reducing noise. In a word, the results provide an effective means for the image processing of moiré fringes.

Keywords Phase information extraction · Gabor wavelet transform · Moiré fringes

1 Introduction

Moiré tomography has become an efficient and important tool in various fields since it was first purposed by O. Kafri [1], because it meets an increasing need for real-time visualization and quantitative measurement of phase objects [2–4]. Up to now, it has been used to diagnose various flow fields, such as flames [2, 5, 6], plasmas [7–9], and supersonic jet flows [4, 10]. In some rare fields, moiré tomography is also effective, including quantifying the scapular motions relative to the thorax [11], improving the measurement accuracy

of multi-LSIs [12], and so on. In summary, for the various measuring objects above, one of the key parameters—phase information which is the basis of subsequent data reconstruction, should be initially focused on.

Up to now, apart from some methods like windowed Fourier transform [13, 14], 2D wavelet transform [15], etc., there are mainly three methods to extract moiré fringes information: the fringe tracking method based on image intensity [16, 17], the Fourier transform method [18–20] and the phase-shifting method [21]. The fringe tracking method uses point-by-point tracking to process the fringe pattern, so it is sensitive to the noise in the image [22]. When there are distortion points in the fringe pattern, the measurement error becomes big, even the measurement result will be wrong, which means fringe tracking method obviously cannot meet the needs of high-precision measurement. Fourier transform and phase-shifting methods can get the whole image information by reconstructing the image phase distribution, and reduce the influence of image defects on the information extraction. Phase-shifting method requires that the measured object keeps steady during the recording process, which requires high mechanical stability of the optical path and the flow field [23]. Although related studies have been used to improve the anti-vibration performance of the phase-shifting method [24, 25], factors such as thermal disturbance of the field still make it unstable in a state. For Fourier transform method, the traditional experimental

✉ Yun-yun Chen
yunqq321@sina.cn

¹ Jiangsu Key Laboratory for Optoelectronic Detection of Atmosphere and Ocean, Nanjing University of Information Science and Technology, Nanjing 210044, China
² Jiangsu Collaborative Innovation Center on Atmospheric Environment and Equipment Technology (CICAEET), Nanjing University of Information Science and Technology, Nanjing 210044, China
³ School of Physics and Optoelectronic Engineering, Nanjing University of Information Science and Technology, Nanjing 210044, China
⁴ Jiangsu International Joint Laboratory on Meteorological Photonics and Optoelectronic Detection, Nanjing University of Information Science and Technology, Nanjing 210044, Jiangsu, China

device can meet its requirements and it can extract the phase information of the entire fringe pattern at one time [20], so it has become the most used method. Although the Fourier transform method has high measurement accuracy, the 2D wavelet transform algorithm has advantages over the Fourier transform method in terms of noise reduction, since the Fourier transform method acts as a global transform of the fringe pattern. [26]. Therefore, maybe the Gabor wavelet transform method could be introduced to extract the phase information of moiré fringes. Previously, the Gabor wavelet transform method has been successfully applied to fringes' phase information extraction in interferometry. For example, Yao Wei applied Gabor wavelet transform to interferogram phase demodulation [27], and J Bethge utilized it to extract phase information in spectral interferometry [28]. However, nobody has tried to use Gabor wavelet transform to extract the phase information of moiré fringes, which will be realized in this study.

In this paper, Gabor wavelet transform is used to extract phase distribution of moiré fringes. The filtering property of Gabor wavelet transform is analyzed, and the phase of moiré fringes is deduced with Gabor wavelet transform. The process of choosing light intensity and deriving the phase is described as well. Then the detail of experiment set-up and its result are introduced. While in the next part, the phase information is successfully extracted with Gabor wavelet transform whose result is compared with that of Fourier transform. Finally, phase information is discussed and analyzed.

2 Theory and derivation

2.1 Moiré fringe intensity distribution selection

The moiré fringes can be seen as the result of multi-shearing interference [29]. Thus, compared with the zero-order filtering, the first-order filter which consists of only two major frequency spectra is more accurate. The frequency spectra of the first-order filter meet $m + n = 1$ or $m + n = -1$, where m and n mean the diffraction orders of the two gratings, respectively. The only difference between the two cases is the sign of phase value, which has no impact on result. In this letter, the case $m + n = 1$ is used to figure out the phase information.

2.2 Phase deduction

When the distance between the two gratings equals to the Talbot distance, the light intensity distribution of +1 filter is described as [29]:

$$I(x, y) = 2a_0^2 a_1^2 + 2a_0^2 a_1^2 \cos \left[\frac{4\pi}{d} y \sin \frac{\alpha}{2} + \phi(x, y) \right], \quad (1)$$

where a_0 and a_1 are the coefficients of the first two terms of Taylor expansion, respectively, $\frac{\alpha}{2}$ is the angle between the grating and the y -axis, $\phi(x, y)$ is the phase.

Removing the direct current component, $4\pi \sin(\alpha/2)/d$ is set as f , so Eq. (1) could be simplified like:

$$I(x, y) = 2a_0^2 a_1^2 \cos [fy + \phi(x, y)], \quad (2)$$

Moreover, Eq. (2) could be written as:

$$I(x, y) = 2a_0^2 a_1^2 [c(x, y) \cos (fy) + s(x, y) \sin (fy)], \quad (3)$$

where $c(x, y)$ and $s(x, y)$ are intermediate quantities set-up for the convenience of calculation, and they meet:

$$c^2(x, y) + s^2(x, y) = 1, \quad (4)$$

$$\phi(x, y) = -\tan^{-1} \left[\frac{s(x, y)}{c(x, y)} \right]. \quad (5)$$

According to Ref. [30], 2D Gabor wavelet transform to moiré fringes intensity distribution should be expressed as:

$$G_{mn}[I(x, y)] = h_{mn}(x, y) * I(x, y), \quad (6)$$

where the symbol $*$ represents a convolution of $h_{mn}(x, y)$ and $I(x, y)$, while $h_{mn}(x, y)$ means Gabor wavelet function as [27]:

$$h_{mn}(x, y) = g(x, y) \exp [2\pi j(U_m x + V_n y)], \quad (7)$$

$$g(x, y) = \left(\frac{1}{2\pi \lambda \sigma^2} \right) \exp \left[-\frac{(x/\lambda)^2 + y^2}{2\sigma^2} \right], \quad (8)$$

where σ is scale factor, and λ represents the sine function wavelength.

In further, $h_{mn}(x, y)$ can be seen as a band-pass filter whose central frequency is (U_m, V_n) , so it can be viewed as that the image is filtered by a channel Gabor filter with a central frequency of $(0, f)$. According to Euler formula, $h_{mn}(x, y)$ could be divided into real ($h_r(x, y)$) and imaginary ($h_i(x, y)$) parts, which is defined by:

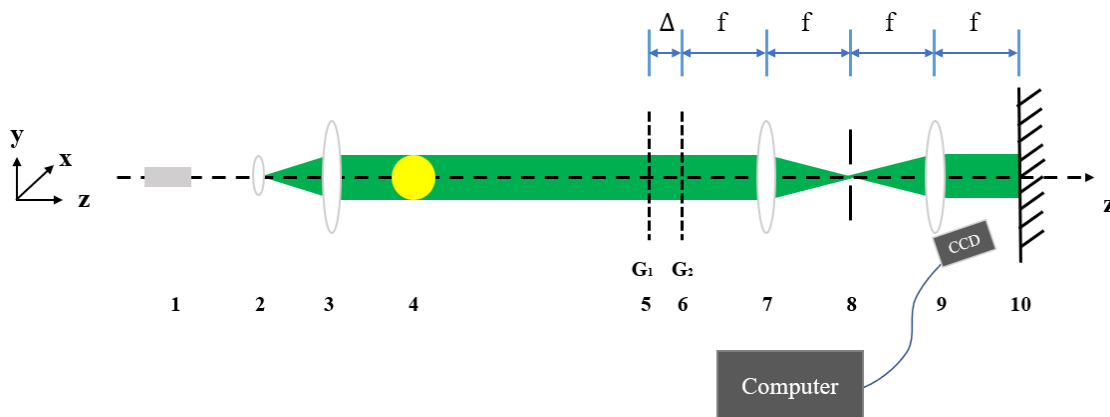
$$\begin{aligned} h_r(x, y) &= g(x, y) \cos (fy), \\ h_i(x, y) &= g(x, y) \sin (fy). \end{aligned} \quad (9)$$

Furthermore, $h_r(x, y)$ and $h_i(x, y)$ are applied to $I(x, y)$ by Gabor wavelet transform, which means doing convolution to the real and imaginary parts separately, we can have:

$$G_{(0,f)}[I(x, y)] = k_r(x, y) + jk_i(x, y). \quad (10)$$

where $k_r(x, y) = h_r(x, y) * I(x, y)$, and $k_i(x, y) = h_i(x, y) * I(x, y)$.

Thus, the phase of $G_{(0,f)}[I(x, y)]$ should be:



1-Laser, 2,3-Beam expanding collimation system, 4-Phase object, 5,6-Ronchi grating, 7,9-Imaging lens, 8-Filter aperture, 10-Screen

Fig. 1 Schematic diagram of moiré deflectometry. 1—laser, 2, 3—beam expanding collimation system, 4—phase object, 5, 6—Ronchi grating, 7, 9—imaging lens, 8—filter aperture, 10—screen

$$\varphi(x, y) = \tan^{-1} \left[\frac{k_t(x, y)}{k_r(x, y)} \right] = fy - \tan^{-1} \left[\frac{g(x, y) * s(x, y)}{g(x, y) * c(x, y)} \right]. \tag{11}$$

As a result of that $\varphi(x, y)$ has the characteristics of the low frequency and narrow-band, as long as the spatial scale chosen for $g(x, y)$ is small enough and should be broad enough to include $\varphi(x, y)$, $\varphi(x, y)$ can be considered to be a constant within the spatial span of $g(x, y)$. Therefore, $c(x, y)$ and $s(x, y)$ can also be seen as constants. Based on these conditions above, an approximation is given as:

$$\frac{g(x, y) * s(x, y)}{g(x, y) * c(x, y)} \approx \frac{s(x, y)}{c(x, y)}. \tag{12}$$

Finally, integrating Eq. (5), Eq. (11) and Eq. (12), the phase distribution $\varphi(x, y)$ can be calculated by:

$$\varphi(x, y) \approx \tan^{-1} \left[\frac{k_t(x, y)}{k_r(x, y)} \right] - fy. \tag{13}$$

The same result can be obtained with the moiré fringes under -1 filter.

3 Experiment and results

3.1 Experimental set-up

Figure 1 is the schematic diagram of moiré deflectometry. In this study, the wavelength of the laser used is 532 nm.

The little lens 2 with the focal length of 3 mm and the large lens 3 with the focal length of 30 cm constitute a beam expanding and collimating system, and the diameter of lens 3 is 5 cm. 5 and 6 are two identical Ronchi gratings, with an effective size of 50 mm × 50 mm, they are set with a distance Δ apart and oriented at angles $\alpha/2$ and $-\alpha/2$ relative to the y-axis, respectively. To obtain the moiré fringes with good contrast, the distance between the two gratings should be the integer multiple of Talbot distance. The imaging lens 7 is the same as the imaging lens 9, and has a diameter and a focal length of 75 mm and 300 mm, respectively. From the back surface of the second grating to the screen is a typical 4-f system. Finally, a CCD is used to obtain moiré fringes.

3.2 Experimental results

In flow fields moiré tomography diagnosis, species composition [31] and flow velocity of jet flow [32] could affect finally results. Therefore, three flow fields are chosen for experiment.

3.2.1 Electric iron

Figure 2 shows the moiré fringes of the flow field around electric iron. The feature of the flow field around electric iron is that when it is heated, there is no chemistry reaction and that the effect of flow velocity can be ignored.

3.2.2 Candle-air flame

Figure 3 shows the moiré fringes of candle burning silently in the air, thus the flow velocity can be ignored. But unlike the flow field around electric iron, there is chemistry reaction of the candle-air flame.

3.2.3 Propane-air flame

The moiré fringes of propane-air flame are given in Fig. 4. Different from both flow fields above, there exists chemistry reaction and the flow velocity is bigger in this case.

4 Phase extraction

4.1 Result of Phase Extraction

The following processing is based on the pre-processing that the moiré fringes image is cut into a 320*320 pixel size. And, the multi-grid method [33] is used to unwrap the phase in this study. Finally, the unwrapped phase information distributions of the three measured flow fields are shown in Figs. 5, 6, 7, and the results based on Fourier transform are also supplied for comparison.

To show the phase information more intuitively, the radial phase distributions are shown in Fig. 8, and the selected sampling diameters are marked in Figs. 5, 6, 7.

Fig. 2 Moiré fringes of electric iron: **a** unheated, **b** heated

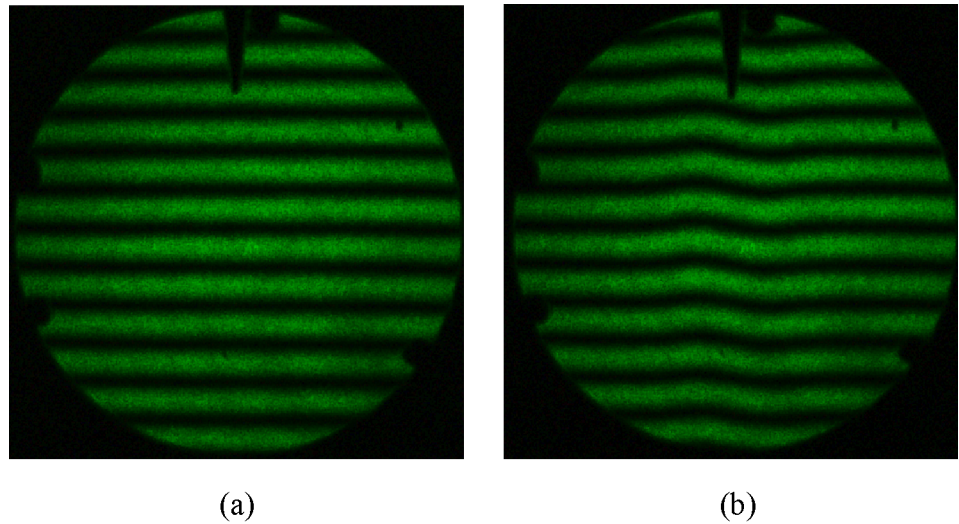


Fig. 3 Moiré fringes of candle-air flame: **a** unburned, **b** burning

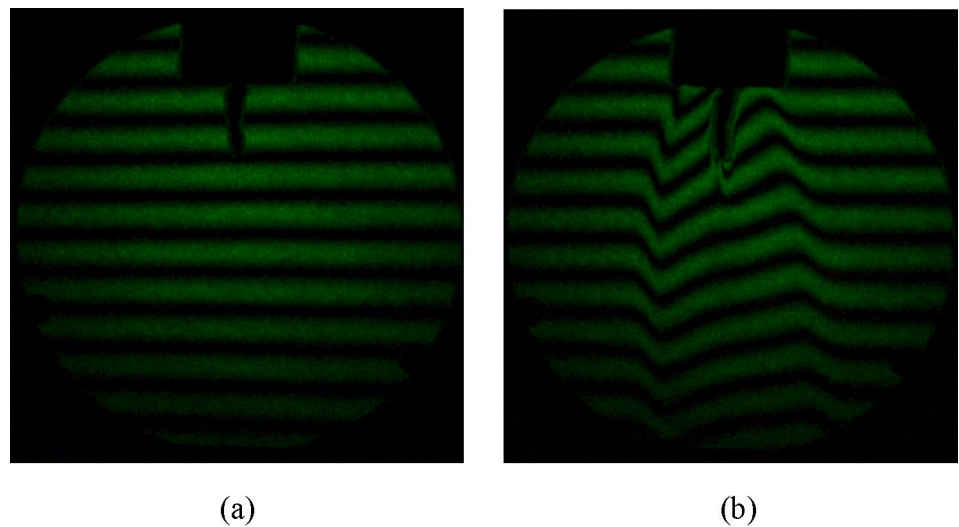


Fig. 4 Moiré fringes of propane-air flame: **a** unburned, **b** burning

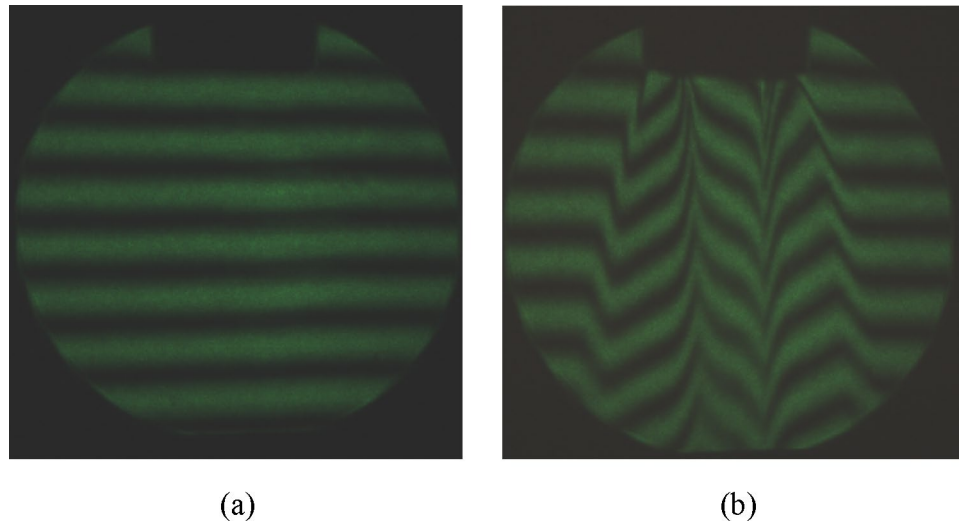


Figure 8 indicates that compared to the phase information extracted with Fourier transform, regardless of the flow field type, the one with Gabor wavelet transform is smoother and the noise is efficiently eliminated.

4.2 Comparison and discussion

As is shown in Figs. 5, 6, 7, 8, comparing the phase information extracted by Gabor wavelet transform with those by Fourier transform, the edge is clearer and the influence of noise is obviously eliminated with Gabor wavelet transform, which could also be seen in Fig. 8. Concretely speaking, the image will be smooth with the real part, while the imaginary part is used to detect

the edge [34] based on filtering by Gabor wavelet transform.

Furthermore, because convolution is involved, the size of the convolution kernel needs to be considered. In the program, the kernel size is an important factor. Image convolution is the process of continuous multiplication and summation when the convolution kernel slides through the pixels on the image line by line. Consequently, if the kernel size is too small, the noise in the image will not be effectively eliminated. However, if the kernel size is too big, various valid information will be filtered out and the accuracy will be reduced. Hence, the optimal value for the kernel size should be considered in two aspects: guaranteed accuracy and noise reduction. To verify how

Fig. 5 Phase information of electric iron: **a** Gabor wavelet transform with kernel size = 30 and $\sigma = 8$, **b** Fourier transform

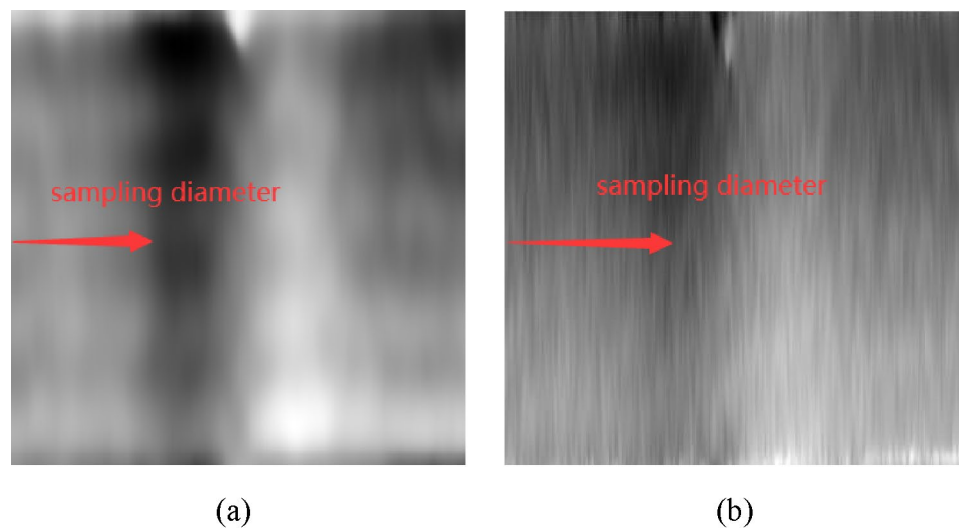


Fig. 6 Phase information of candle-air flame: **a** Gabor wavelet transform with kernel size = 50 and $\sigma = 8$, **b** Fourier transform

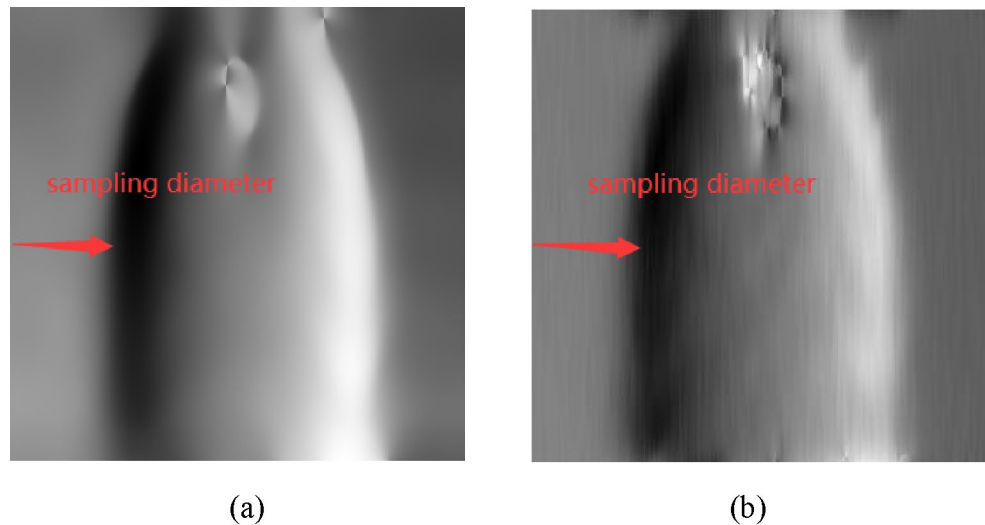
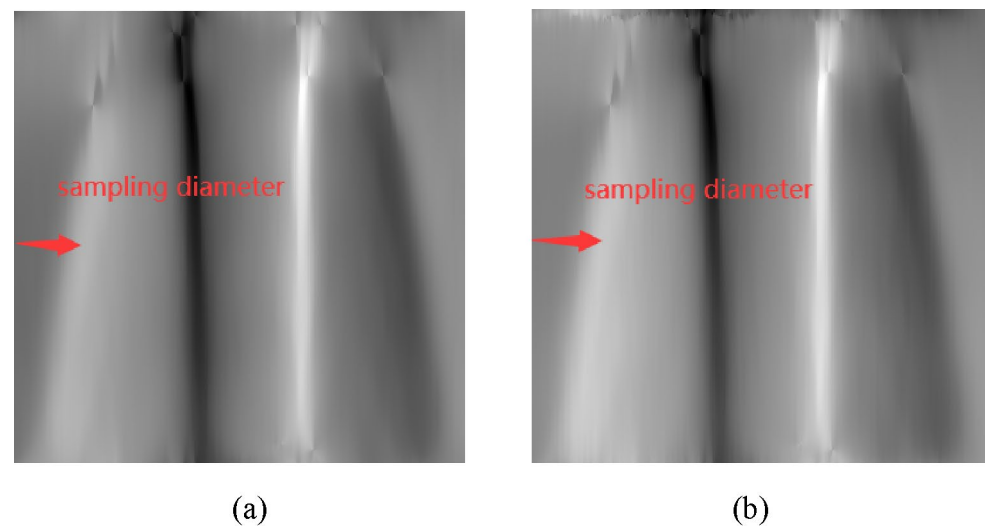


Fig. 7 Phase information of propane-air flame. **a** Gabor wavelet transform with kernel size = 2 and $\sigma = 8$, **b** Fourier transform



the kernel size affects the extracted phase result, one set of images is shown.

Figure 9 shows the reconstructed phase of three different flow fields with the same kernel size, and the edge clarity of the three phase images is different. Obviously, the phase of electric iron and candle-air flame are basically normal, but the edge of propane-air flame's phase is distorted seriously. It is because that compared with the other two cases, the propane-air flame's phase has two peaks, and that the information is denser at the inflection point, the kernel size should be as small as possible to

ensure its accuracy. Thus, the most suitable kernel size for propane-air flame is 2 in the actual operation of the program, as is shown in Fig. 7a, which is better than that shown in Fig. 9c.

As a comparison, the edges of candles and soldering irons are much smoother, so the kernel size of them could be bigger. Apparently, even if the kernel size is chosen as 50, it is still appropriate for both the electric iron and candle-air flame. Therefore, regarding different flow fields, the optimal value for the kernel size should be different.

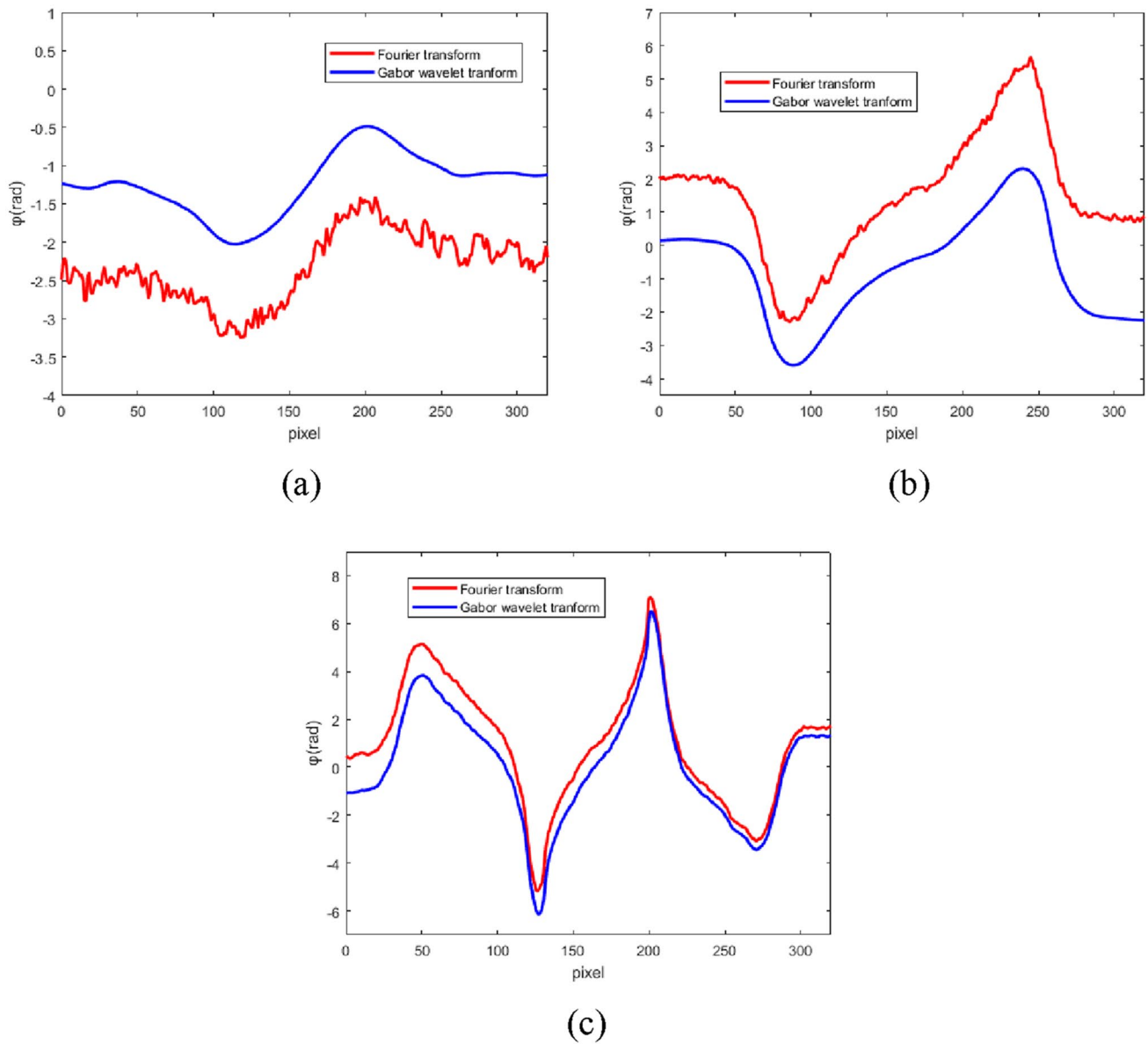


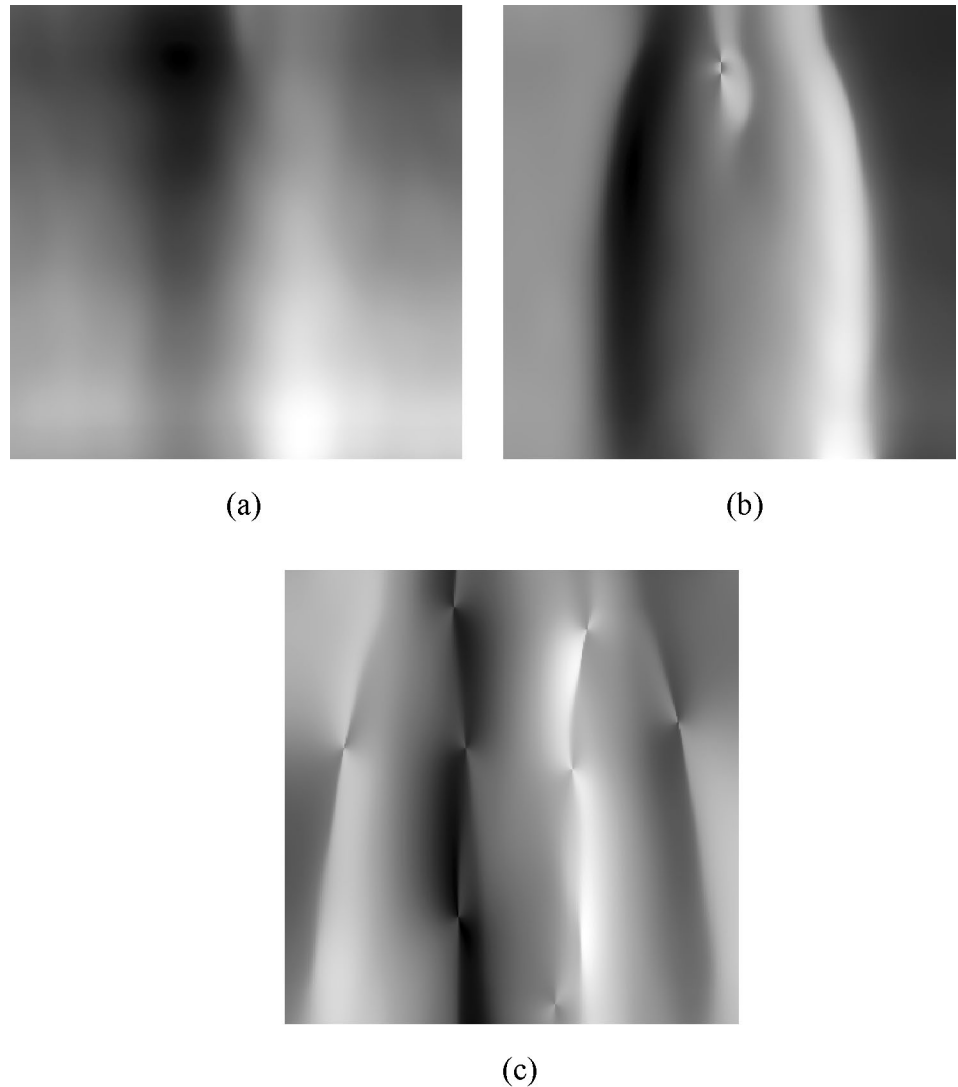
Fig. 8 Radial distribution of phase information: **a** electric iron, **b** candle, **c** propane

Furthermore, for the sake of proving the effect of kernel size on final phase information, Fig. 10 is supplied. And the candle-air flame is chosen for further discussion.

Figure 10 shows the phase information of candle-air flame extracted with the kernel sizes at 10, 50, and 100, respectively. It demonstrates that as the kernel size increases, the image

of phase distribution becomes smoother. However, when the value of kernel size exceeds a specific value, the edge of the image becomes strange which means that the accuracy deduces.

Fig. 9 Phase information at the same kernel size of 50: **a** Electric iron, **b** candle-air, **c** propane-air

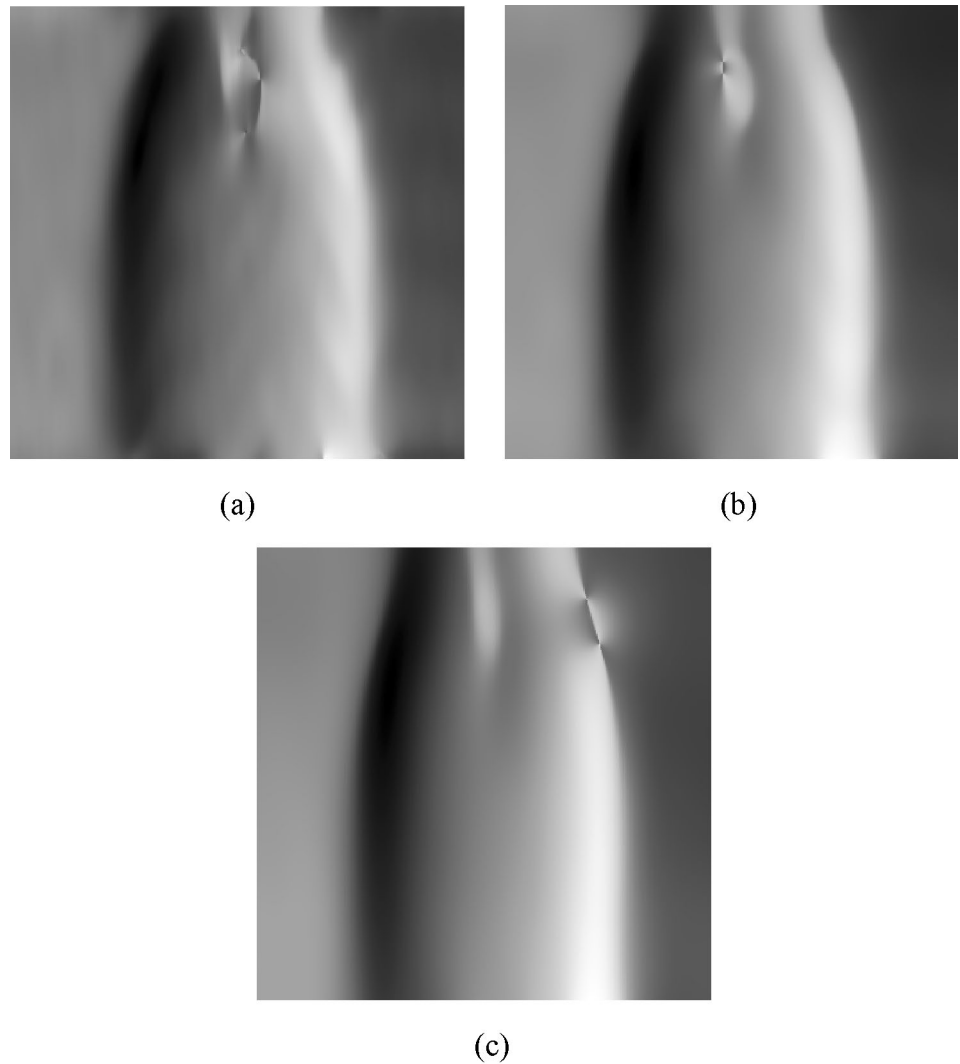


5 Conclusion

In this paper, it is proved that Gabor wavelet transform is an excellent method to extract the phase information of moiré fringes. First, the expression of moiré fringes phase is derived theoretically. In the process above, Gabor wavelet function acts as a band-pass filter. Then, the moiré fringes of three typical flow fields are obtained

by experiment. Based on which, the phase information is extracted with Gabor wavelet transform. Compared with the phase results extracted with Fourier transform, the effect of noise is efficiently eliminated, and the entire phase distribution is more accurate. Finally, the influence of the kernel size is discussed, which manifests that a proper kernel size can promote both the smoothness and the accuracy of phase distribution.

Fig. 10 Phase information of candle-air flame extracted with different kernel sizes: **a** 10, **b** 50, **c** 100



Acknowledgements This work was funded by the National Natural Science Foundation of China (Grant No. 61975083), and the research, innovation plan for Postgraduates for Jiangsu Province (No. KYCX21_0986), and the Innovation and Entrepreneurship Training Program for College Students of Jiangsu Province (Grant No. 202110300038Z).

References

1. Kafri, O.: Noncoherent methods for mapping phase objects. *Opt. Lett.* **5**(12), 555–557 (1980)
2. Posner, J.D., Dunn-Rankin, D.: Temperature field measurements of small, nonpremixed flames with use of an Abel inversion of holographic interferograms. *Appl. Opt.* **42**(6), 952–959 (2003)
3. Wan, X., Yu, S., Cai, G., Gao, Y., Yi, J.: Three-dimensional plasma field reconstruction with multiobjective optimization emission spectral tomography. *J. Opt. Soc. Am. A* **21**(7), 1161–1171 (2004)
4. Hemanth, T., Mohan, R.V., Rajan, K.: Quantitative flow visualization in supersonic jets through tomographic inversion of wavefronts estimated through shadow casting. *Appl. Opt.* **45**(20), 5010–5019 (2006)
5. Juste, G.L., Contat-Rodrigo, L.: Temperature field reconstruction from phase-map obtained with moiré deflectometry in diffusion flame on solids. *Combust. Sci. Technol.* **179**(7), 1287–1302 (2007)
6. Ibarreta, A.F., Sung, C.J.: Flame temperature and location measurements of sooting premixed Bunsen flames by rainbow Schlieren deflectometry. *Appl. Opt.* **44**(17), 3565–3575 (2005)
7. Chen, Y.Y., Song, Y., Li, Z.H., He, A.Z.: A model for arc plasma's optical diagnosis by the measurement of the refractive index. *Opt. Commun.* **284**(12), 2648–2652 (2011)
8. Salimi Meidanshahi, F., Madanipour, K., Shokri, B.: Measurement of temperature and electrons density distribution of atmospheric arc plasma by moiré deflectometry technique. *Opt. Lasers Eng.* **51**(4), 382–387 (2013)
9. Chen, Y.Y., Song, Y., Gu, F., Shao, S.F., Zhang, Y.Y.: High temperature flow field's electron number density measurement by two-wavelength moiré tomography. *Opt. Lett.* **41**(7), 1640–1643 (2016)
10. Song, Y., Zhang, B., He, A.Z.: Algebraic iterative algorithm for deflection tomography and its application to density flow fields

- in a hypersonic wind tunnel. *Appl. Opt.* **45**(31), 8092–8101 (2006)
11. Gomes, P.F., Sesselmann, M., et al.: Measurement of scapular kinematics with the moiré fringe projection technique. *J. Biomech.* **43**, 1215–1219 (2010)
 12. Liu, Ke., Ji, Z., Chen, C., Li, Y.: Phase extraction using multi-directional moiré fringes for multi-lateral shearing interferometry. *Opt. Lasers Eng.* **90**, 81–89 (2017)
 13. Zhong, J., Zeng, H.: Multiscale windowed Fourier transform for phase extraction of fringe patterns. *Appl. Opt.* **46**(14), 2670–2675 (2007)
 14. Kemaq, Q., Wang, H., Gao, W.: Windowed Fourier transform for fringe pattern analysis: theoretical analyses. *Appl. Opt.* **47**(29), 5408–5419 (2008)
 15. Watkins, L.R.: Review of fringe pattern phase recovery using the 1-D and 2-D continuous wavelet transforms. *Opt. Lasers Eng.* **50**(8), 1015–1022 (2012)
 16. Servin, M., Rodriguez-Vera, R., Carpio, M., Morales, A.: Automatic fringe detection algorithm used for moiré deflectometry. *Appl. Opt.* **29**(22), 3266–3270 (1990)
 17. Canabal, H., Quiroga, J.A., Bernabeu, E.: Automatic processing in moiré deflectometry by local fringe direction calculation. *Appl. Opt.* **37**(25), 5894–5901 (1998)
 18. Quiroga, J.A., Crespo, D., Bernabeu, E.: Fourier transform method for automatic processing of moiré deflectograms. *Opt. Eng.* **38**(6), 974–982 (1999)
 19. Wang, M.: Fourier transform moiré tomography for high-sensitivity mapping asymmetric 3-D temperature field. *Opt. Laser Technol.* **34**(8), 679–685 (2002)
 20. Zhong, J., Wang, M.: Fourier transform moiré deflectometry for the automatic measurement of phase objects. *Proc. SPIE* **2899**, 311–318 (1996)
 21. Ranjbar, S., Kholesifard, H.R., Rasouli, S.: Nondestructive measurement of refractive index profile of optical fiber preforms using moiré technique and phase shift method. *Proc. SPIE* **6025**, 602520-1–7 (2006)
 22. Quan, C.G., Tay, C.J., Yang, F.J., He, X.Y.: Phase extraction from a single fringe pattern based on guidance of an extreme map. *Appl. Opt.* **40**(23), 4814–4821 (2005)
 23. Yan-Guo, Z., Song, Y., Wang, J., Li, Z.-H., He, A.: Theoretical analysis and experimental verification of six-step spatial phase-shifting shearing interferometry by double gratings. *J. Opt. Soc. Am. A* **30**(8), 1535–1543 (2003)
 24. Koliopoulos, C.L.: Simultaneous phase shift interferometer. *SPIE* **1531**, 119–127 (1991)
 25. Zhao, C., Burge, J.H.: Vibration-compensated interferometer for surface metrology. *Appl. Opt.* **40**(34), 6215–6222 (2001)
 26. Niu, H., Quan, C., Tay, C.J.: Phase retrieval of speckle fringe pattern with carriers using 2D wavelet transform. *Opt. Lasers Eng.* **47**(12), 1334–1339 (2009)
 27. Yao, W., He, A.: Application of Gabor transformation to the two-dimensional projection extraction in interferometric tomography. *J. Opt. Soc. Am. A* **16**(2), 258–263 (1996)
 28. Bethge, J., Grebing, C., Steinmeyer, G.: A fast Gabor wavelet transform for high-precision phase retrieval in spectral interferometry. *Opt. Express* **15**(22), 14313–14321 (2007)
 29. Song, Y., Chen, Y., He, A., Zhao, Z.: Theoretical analysis for moiré deflectometry from diffraction theory. *J. Opt. Soc. Am. A* **26**(4), 882–889 (2009)
 30. Bovik, A.C., Clark, M., Geisler, W.S.: Multichannel texture analysis using localized spatial filters. *IEEE Trans. Pattern. Anal. Mach. Intell.* **12**, 55–73 (1990)
 31. Tieng, S.M., Lin, C.C., Wang, Y.C., Fujiwara, T.: Effect of composition distribution on holographic temperature measurement of a diffuse flame. *Meas. Sci. Technol.* **7**(4), 477–488 (1996)
 32. Chen, Y.-Y., Yang, Yu., Zhong, X., Zhang, Y.-Y.: Influence of flow velocity on flow field's optical tomography diagnosis. *Opt. Commun.* **382**, 386–391 (2017)
 33. Song, Y., Chen, Y.Y., He, A.Z., Zhao, Z.M.: Moiré tomography based on phase reconstruction. *Acta Optica Sinica* **29**(5), 1232–1239 (2009). (in Chinese)
 34. Mehrotra, R., Namuduri, K.R., Ranganathan, N.: Gabor filter-based edge detection. *Pattern Recogn.* **25**(12), 1479–1494 (1992)

Publisher's Note Springer Nature remains neutral with regard to jurisdictional claims in published maps and institutional affiliations.